LA-UR-20-29893
Approved for public release; distribution is unlimited.

Title: Summary of Simulations with Advanced Hydrodynamic Methods Supporting the Ristra Milestone

Author(s): Chiravalle, Vincent P.

Intended for: Report

Issued: 2020-12-23 (Rev.1) (Draft)

Summary of Simulations with Advanced Hydrodynamic Methods Supporting the Ristra Milestone

Vincent Chiravalle (XCP-4)

November 21, 2020

1.0 Introduction

Among the numerical methods that have been exercised within the FLeCSI framework for the Ristra project at LANL are an advanced cell centered hydrodynamic (CCH) method [1] and a finite element staggered grid hydrodynamic (SGH) method [2]. This report describes how these methods have been implemented in Ristra project tools, and evaluates these methods using a series of twelve test problems.

Both the CCH and SGH methods follow a Lagrange plus remap approach and solve a multi-material approximate Riemann problem to find forces and displacements during the Lagrangian phase. The CCH method solves the Riemann problem at the vertices of the cell, while the SGH method solves the Riemann problem at the center of the cell. The Riemann solution introduces dissipation and also dampens unphysical hourglass motion. The amount of dissipation generated by the Riemann solution is controlled using a discrete Mach number or smoothness indicator.

The CCH and SGH methods each include a swept-face multi-material remap [3], that follows closely the method used in FLAG, where materials within a cell are represented as polygons with piece-wise linear interfaces separating distinct materials. The swept-face remap used in the CCH and SGH methods is separate from the remap methods developed for Portage, and is written entirely within the FLeCSI framework. For cells containing multiple materials an interface-aware subscale dynamics (IA-SSD) closure model [4] is available as an option to help drive materials within a cell towards pressure equilibrium. Volume and energy fluxes are exchanges between pairs of materials, with the interface area determined from the material polygons constructed during the prior remap step. The IA-SSD model is essential in order to accurately simulate the Le Blanc shock tube problem with these CCH and SGH methods on an Eulerian mesh.

The CCH and SGH methods were implemented within both the Flecsale-mm and Symphony codes for the Ristra project. This was accomplished by creating separate apps within Flecsale-mm and Symphony, starting from an existing app called Maire_Hydro, and completely replacing the all routines associated with the hydrodynamic update and the equation of state. The CCH and SGH apps created for Flecsale-mm and Symphony have their own custom parser for the input deck, and produce dump files in Ensight Gold format, which can be used for visualization and also as input to restart a simulation. The input deck parser recognizes global parameters, lists of material parameters, lists of boundary conditions, and lists of instructions for setting the initial conditions on logical mesh regions. Materials can be painted onto a portion of the mesh by specifying the coordinates of a polygon.

In addition to the CCH and SGH apps created for Flecsale-mm and Symphony, a stand-alone C++ code called FUEL was created which borrows the overall code structure, routines, and much of the C++ coding from the CCH app in Flecsale-mm and Symphony, but without the FLeCSI framework. FUEL has its own

mesh class, which provides similar functionality as the Burton mesh specialization, and has its own data classes for cell, vertex, and corner data as well. MPI communication is done explicitly within FUEL. When using the same mesh partition and the same number of MPI ranks, FUEL and the CCH app in Flecsale-mm have essentially the same runtime for the 5-material compression problem, a test problem that has both strength and multi-material remap.

For this work the November 2020 branch of Flecsale-mm and the August 2019 branch of Symphony were used to build the CCH and SGH apps, incorporating pre-built third party libraries located in "/usr/projects/ngc/public/symphony" on LANL's Snow HPC machine, with a toolchain consisting of MPICH-3.2.1 and GCC-7.4.0. The same toolchain was used to compile FUEL, with the added simplification that FUEL does not link against any third party libraries. Simulations with Symphony and Flecsale-mm always used a single node of Snow and generally involved the full number of cores on the node, 36 cores, unless otherwise stated. The number of nodes used in the FUEL simulations varied, depending on the problem, but never exceeded the limit of 20 nodes.

In the following sections the CCH and SGH methods are evaluated using a series of tests involving strong shocks, such as the Le Blanc, Sedov, and triple point problems, smooth flows such as the isentropic spherical compression problem, and material strength including the 5-material compression problem, the Verney problem, and a tantalum Taylor anvil experiment. The isentropic spherical compression problem, which is a variant of the Kidder ball problem, was simulated with both the Symphony CCH app and with FUEL. The FUEL simulation involved 10.9 million cells, using 10 nodes of Snow with 360 total processors. The Verney problem was simulated with the Symphony SGH app on a purely Lagrangian mesh, giving excellent agreement with the analytic solution for the internal energy of the collapsing shell. The Taylor anvil problem was simulated with both Flecsale-mm and FUEL, using the SGH method, modified to include the VPSC crystal plasticity model [5]. The FUEL simulation of the Taylor anvil involved 20 nodes of Snow with 520 total processors. The Symphony CCH and SGH apps were compared when calculating the 5-material compression problem on an Eulerian mesh. A 1.35 million zone Eulerian simulation of the 5-material problem was also conducted using FUEL, involving 10 nodes of Snow with 360 processors. Finally a tin pulsed power experiment was simulated with both Flecsale-mm and FUEL. This problem uses a 2D trilink file to initialize the 3D simulation in either Flecsale-mm or FUEL, and like the 5-material compression problem also includes material strength and multi-material remap on an Eulerian mesh. The simulated geometry of the compressed tin target is compared against the experimental proton radiographs.

2.0 Le Blanc shock tube

The Le Blanc shock tube problem involves a strong initial discontinuity between two materials, each having an ideal gas equation of state (γ= 5/3). The total length of the shock tube is 9 cm and the initial interface between the two materials is located at 3 cm. The high pressure material has an initial density of 1 g/cm^3 and a specific internal energy of 0.01 MJ/g, while the lower pressure material has an initial density of 0.001 g/cm^3 and a specific internal energy of 10^{-8} MJ/g. Calculated values of density and

internal energy at 6.0 μs are shown in Fig.1 using the CCH app in Symphony. Results on a fixed Eulerian mesh using the IA-SSD closure model are shown in red. For this Eulerian simulation, the computational mesh consists of 720 by 1 by 1 cells, with the cells distributed in a spatially uniform manner and with nodal positions that are fixed at all times during the simulation. A Lagrangian simulation, shown in blue, was also performed on a mesh consisting of 1280 by 1 by 1 cells, with 80 cells in the low density region.

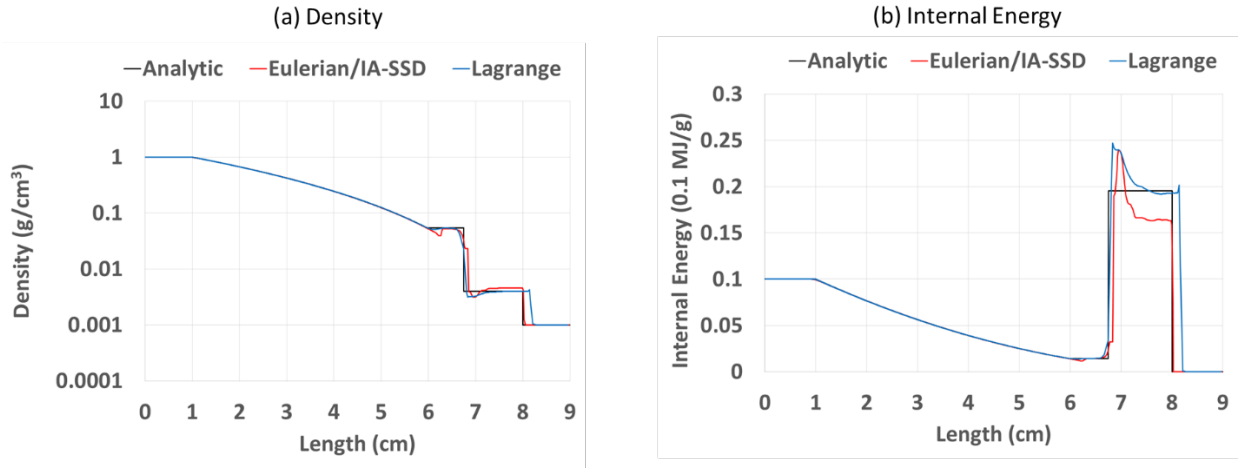

Figure 1. Calculated density (a) and specific internal energy (b) for the LeBlanc shock tube problem at 6.0 μs, using the CCH app in Symphony. Results from the Symphony CCH app on a fixed Eulerian mesh using the IA-SSD closure model (red), and from the Symphony CCH app on a purely Lagrangian mesh (blue). The solid black line represents the analytic solution.

The Eulerian simulation captures the shock at about 8 cm and does a good job representing the expansion fan, as indicated in Fig. 1(b). However the calculated contact surface is located at 6.84 cm, which is slightly ahead of the analytic solution at 6.75 cm. Furthermore, the Eulerian simulation produces less internal energy immediately behind the shock and generates more internal energy at the contact surface relative to the analytic solution. The Lagranian simulation produces the correct amount of internal energy at the shock front, but the calculated location of the shock front is slightly ahead of the analytic solution.

3.0 Isentropic Spherical Compression

The isentropic spherical compression problem is a variant of the Kidder ball problem with an initial Gaussian density profile. The isentropic spherical compression problem involves an ideal gas (γ= 5/3) with the following initial conditions: a linear velocity field, a Gaussian density profile, and a constant specific internal energy. Ramsey et. al. [6] derived a self-similar solution for this problem that has a spatially-uniform but time-varying specific internal energy.

The boundary conditions include three planes of symmetry encompassing the origin, and an outer boundary that moves according to the analytic solution. This problem is simulated with the outer boundary internal to the mesh and with a separate material region outside that boundary, which enables this calculation to be run Eulerian. The inner material is an ideal gas consisting of a 3 cm cube where the initial conditions are prescribed as discussed above. The outer material is also an ideal gas, but with zero velocity and unit density, occupying a region that extends outward by 0.3 cm in each direction relative to the volume occupied by the first material. A 44 by 44 by 44 Eulerian mesh was used for the simulation.

The goal is to assess the formal accuracy of the Symphony CCH app over the inner material region to a radius of 2 cm. The volume fraction of the inner gas region is displayed in Fig. 2(a), and the corresponding density contours are shown in Fig. 2(b). All cell-centered values of density from the simulations at 0.5 μs, within a radius of 2.0 cm from the origin, are shown in Fig. 3, revealing excellent agreement between the analytic solution and the computed result. Near the origin, the Symphony CCH simulation lies nearly on top of the analytic solution even at the low spatial resolution used here.

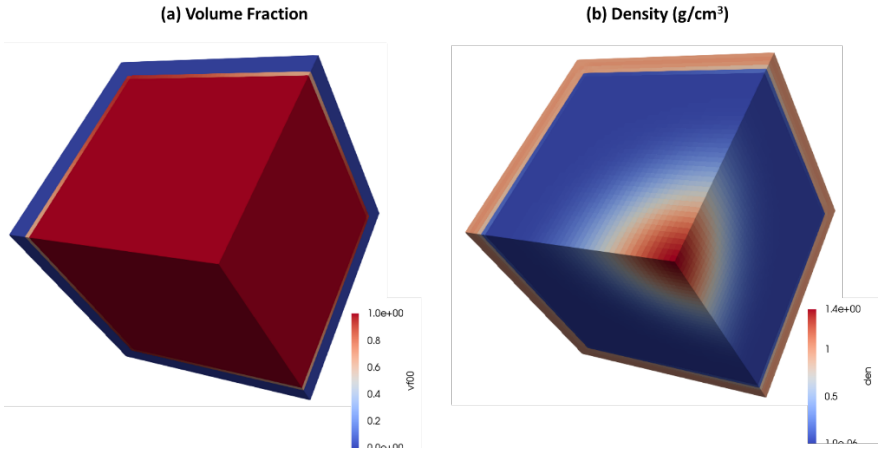

Figure 2. Results from the Symphony CCH app for the isentropic spherical compression problem at t=0.5 μs on a 44 by 44 by 44 mesh, showing (a) volume fraction and (b) density.

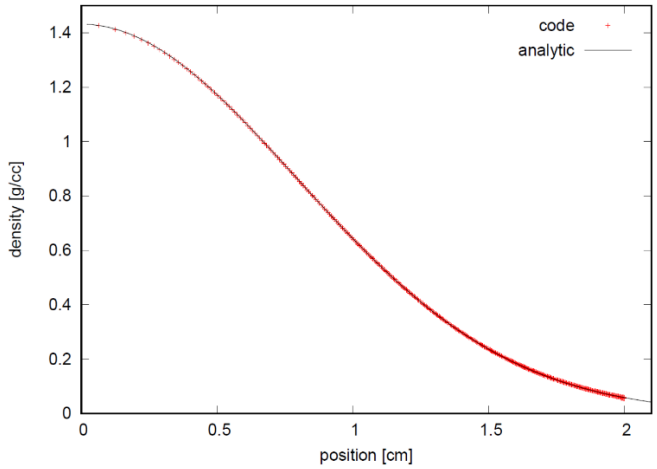

Figure 3. Cell-centered values of density (red) from the Symphony CCH solution. The analytic solution is given in black.

Corresponding results using FUEL with a more finely resolved 176 by 176 by 352 mesh consisting of 10.9 million zones are presented in Figure 4. This simulation was performed using 320 processors on 10 nodes of Snow. The simulation was initialized at t=0 using a link file containing 2D triangular elements, which FUEL read and then rotated to create a 3D mesh.

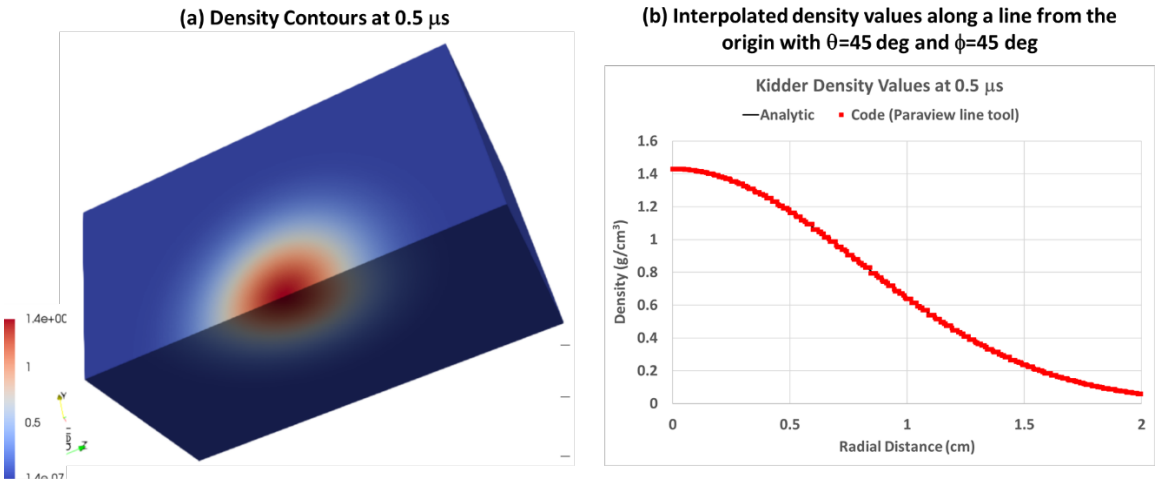

Figure 4. FUEL simulation results for the isentropic spherical compression problem at t=0.5 μs using a 10.9 million zone mesh: full density contours (a) and density along a line at a solid angle of 45 degrees (b).

4.0 Sedov

The 3D Sedov blast wave problem provides a stringent test for assessing the accuracy and robustness of a hydrodynamic algorithm. An ideal gas (γ=5/3) is used with an initial energy source of 56 kJ at the origin represented by a single cell, which is treated as a distinct material in these simulations. The

physical domain encompasses a 1.2 cm square octant which is represented by a computational mesh having 40 by 40 by 40 cells. This problem was simulated using an Eulerian mesh with the nodal positions fixed at all times.

The volume fraction and density simulated with the Symphony CCH app are shown in Fig. 5 at 1.0 μs. The symmetry of the calculated blast front is excellent considering this level of resolution. The cell near the origin where the energy source was deposited has expanded substantially during the 1.0 μs time interval of the calculation, which is evident by the volume fraction shown in Fig. 5(a). The multi-material remap and associated interface reconstruction algorithm adequately represent the two materials in the problem. Despite the fact that the multi-material remap does not conserve total energy, the calculated location of the shock front is captured fairly well when compared to the analytic solution as shown in Fig. 6.

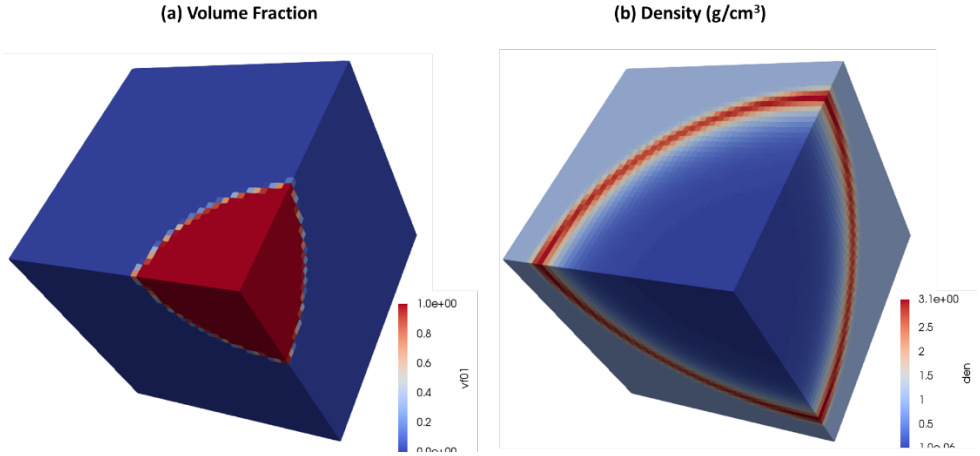

Figure 5. Results with the Symphony CCH app for the Sedov problem at t=1.0 μs on a 40 by 40 by 40 mesh, showing (a) volume fraction and (b) density.

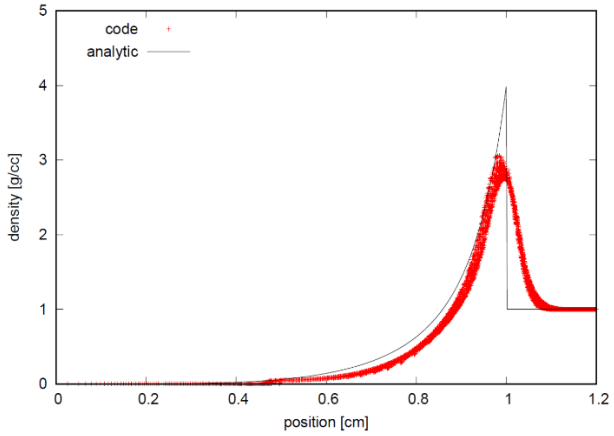

Figure 6. Cell centered values of density (red) from the Symphony CCH solution of the Sedov problem. The analytic solution is given in black.

5.0 Triple Point

The triple-point problem is a test problem that generates significant vorticity. There are two materials in the problem which are ideal gases, and three regions with distinct initial conditions as illustrated in Fig. 7. The first high pressure region and the low pressure region have g=1.5, while the second high pressure region has γ=1.4. The first high pressure region is 1 cm in length (along x-axis) and 3 cm in width (along y-axis) with an initial density of 1 g/cm^3 and an initial pressure of 1 Mbar. Adjacent to this region are two separate regions both 6 cm in length. One of these regions is a high pressure gas that extends 1.5 cm outward from the y-axis and has the same initial pressure but an initial density of 0.1g/cm^3. Above the second high pressure region is a low pressure region with an initial pressure of 0.125 Mbar and density of 0.1 g/cm^3. A vortex develops at the point where all three regions meet. A fixed Eulerian mesh with 210 by 90 by 2 cells was used for simulations with the Flecsale-mm CCH app.

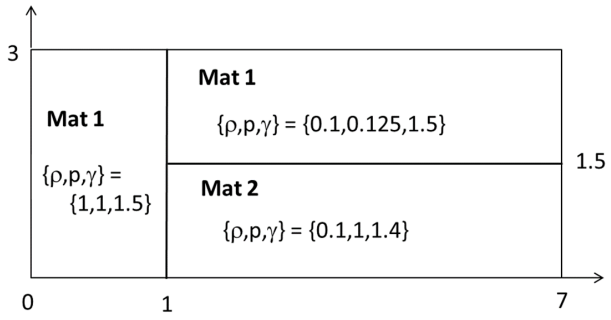

Figure 7. Geometry and initial conditions for the triple point problem with two materials and three regions. For each region the initial values of density (g/cm^3), pressure (Mbar), and ideal gas γ are given in brackets.

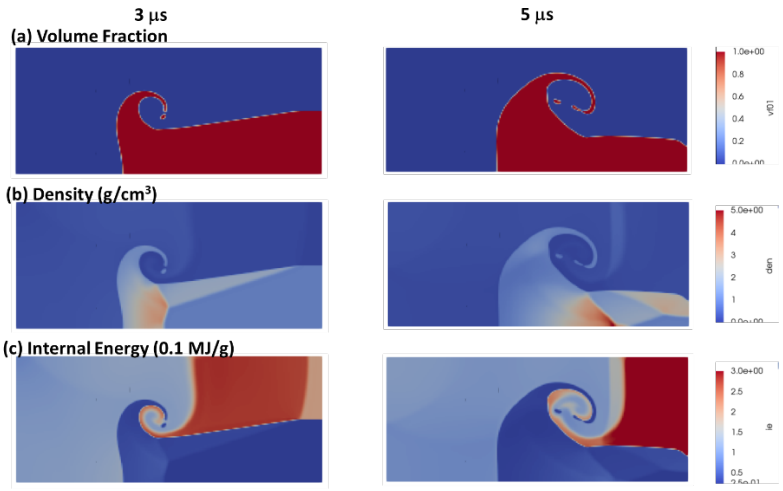

Figure 8. Flecsale-mm CCH results for the triple point problem on a fixed Eulerian mesh at 3 μs and 5 μs: (a) volume fraction, (b) density, and (c) internal energy contours.

The calculated density and internal energy for the triple point problem at 3 μs and 5 μs are given in Fig. 8, using the Flecsale-mm CCH app. The calculated solution includes two prominent features - a vortex and a Mach stem respectively. The vortex is created by a Kelvin-Helmholtz instability in the physical flow. The amount of rotation at the tip of the vortex is sensitive to the resolution of the numerical simulation and the amount of dissipation introduced by the hydrodynamic algorithm. Below the vortex, two shocks interact to create a Mach stem. The Mach stem is fully developed at 5 μs and has a peak density of about 5 g/cm^3.

6.0 Bubble Collapse

With the bubble collapse test problem [4], the ability of the Flecsale-mm CCH app to simulate the closure of a bubble cavity by a shock wave is evaluated. The domain has physical extents of

$$(x, y, z) \in [-1.5: 1.5] \times [-0.5: 0.5] \times [0: 0.025].$$

The mesh is Eulerian and all boundaries are walls. The bubble, which is a distinct material in the problem, is centered at the origin with a radius of 0.3 cm and an initial density of 10^{-3}. The rest of the domain is a separate material in the problem, consisting of two regions of ideal gas as follows:

$$\rho = 1, \quad p = 10^5, \qquad u = (0,0,0) \qquad x > -0.5$$

$$\rho = 4, \quad p = 1.334, \quad u = (1,0,0) \qquad x < -0.5.$$

This generates a shock wave, with the front located initially at x = -0.5 cm. The shock is moving to the right. The volume fraction of the bubble at several times during its collapse is shown in Fig. 9. At 0.3 μs the bubble has the shape of a crescent moon and is almost completely collapsed by 0.4 μs. However the bubble does not entirely disappear, evident by the tiny pockets of bubble material that remain at 0.9 μs shown in Fig. 9 (a). The Flecsale-mm CCH app produces a peak density of about 10 g/cm^{-3} at the shock front at 0.9 μs, as shown in Fig. 9 (b).

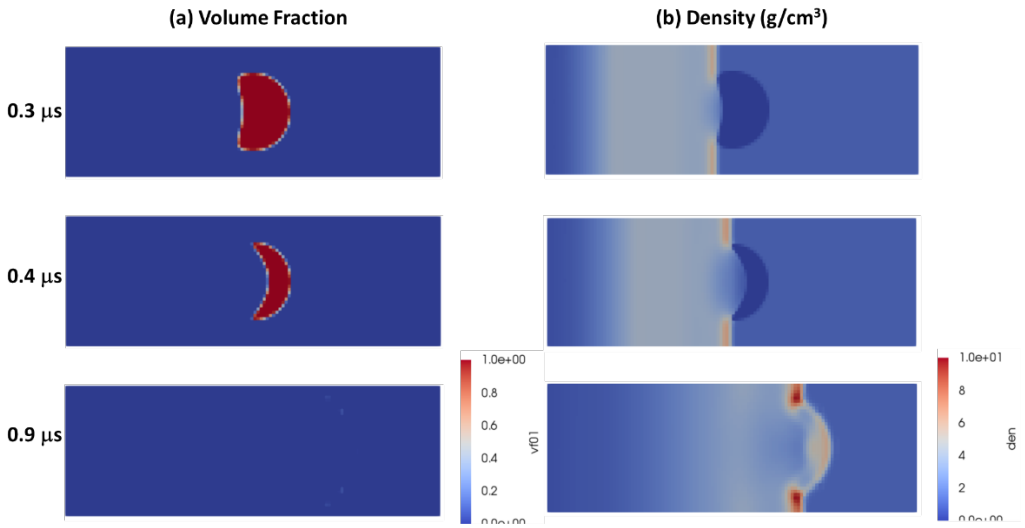

Figure 9. Flecsale-mm CCH results for the bubble collapse test problem at three different times: (a) volume fraction and (b) density.

7.0 Plate Impact

A simplified projectile-plate impact problem [4] in the $(x, y, z) \in [0: 2] \times [0: 2] \times [0: 0.025]$domain. An 80 by 80 by 2 computational mesh is used for the simulations of this problem with the Flecsale-mm CCH app on an Eulerian mesh. There are three materials in the simulation, background gas, projectile and plate, and all of these materials are modeled as ideal gases with different properties:

background-gas: $\gamma = \frac{5}{3}, \quad \rho = 10^{-3}, \; u = (0,0,0)$

projectile: $\gamma = 50, \; \rho = 20, \quad u = (0.2,0.05,0)$

plate: $\gamma = \frac{5}{3}, \quad \rho = 15, \quad u = (0,0,0)$

The initial pressure is set to 10^{-7} everywhere, and the deviatoric stress is set to zero at all times during the simulation. The projectile is defined by a polygon in the (x,y) plane with vertices:

$$(x, y) \in \big((0.225,0.7), (0.725,0.825), (0.675,1.025), (0.175,0.9)\big).$$

This problem was simulated on an Eulerian mesh using the Flecsale-mm CCH app. Density contours within the projectile and plate are presented in Fig. 11. The projectile impacts the plate at about 1.5μs, and at 6.0 μs the projectile has moved completely through the plate. The initial value of density (20 g/cm^3) within the projectile is maintained fairly well during the simulation. The density in the expanding plate region at 6.0 μs is generally between 0.4 g/cm^3 and 1.2 g/cm^3.

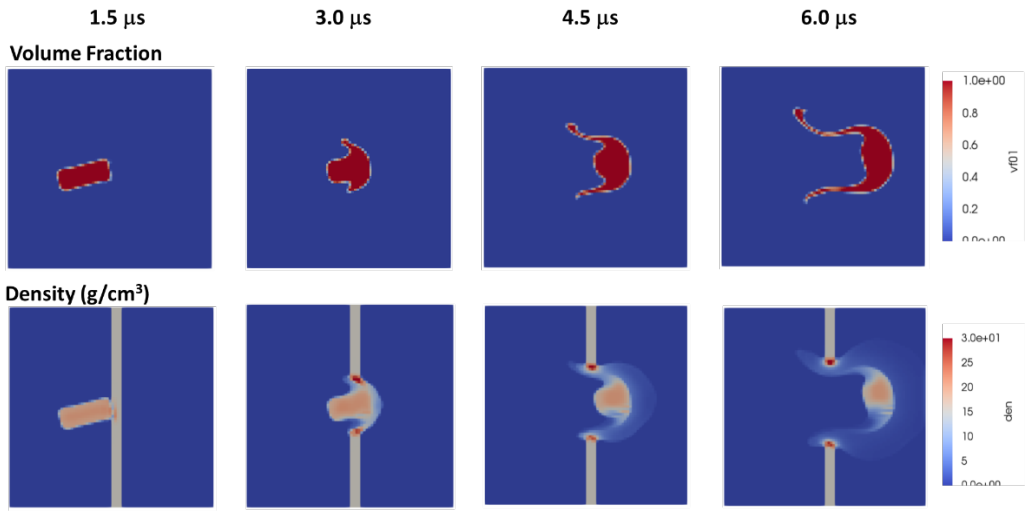

Figure 10. Results for the plate impact problem using the Flecsale-mm CCH app at various times during the simulation: (a) volume fraction of the projectile and (b) density.

8.0 Simplified Shaped-Charge Problem

The focus of this section is a simplified shaped-charge problem [4] that uses a simplified set of materials but shows some of the features of real shaped-charge experiments. There are three materials in the problem, a "high explosive", a "shell", and background gas. All of these materials are represented as ideal gases with the following properties:

high explosive: $\gamma = 1.4, \quad \rho = 1, \quad p = 10^{-7}$

shell: $\gamma = 50, \quad \rho = 10, \quad p = 10^{-7}$

background-gas: $\gamma = 5/3, \quad \rho = 10^{-3}, \quad p = 10^{-7}$

The domain occupied by the "high explosive" is defined by a polygon with the following (*x,y*) vertices:

(-1.0,-0.5), (2.5,-0.5), (0.0, 0.0), (2.5, 0.5), (-1.0, 0.5);

the shell domain is defined by a polygon

(2.5,-0.5), (3.0,-0.5), (0.5, 0.0), (3.0, 0.5), (2.5, 0.5), (0.0, 0.0);

and the rest is filled with background gas:

(3.0,-0.5), (5.0,-0.5), (5.0, 0.5), (3.0, 0.5), (0.5, 0.0).

The boundaries of the domain are walls. Calculations are performed on 120 by 20 by 2 cell mesh. There is a high value of internal energy, *e*=2.5e5 MJ/g, in the two cells in the "high explosive" that are located adjacent to the left boundary at its center. This initial energy source produces pressures as high as 10 GBar in the "high explosive" and "shell" materials during the formation of the jet. Since the peak pressure is much higher than in a real shaped-charge the formation of the jet takes place on a much shorter time scale on the order of nanoseconds.

The simplified shaped charge problem was simulated with Flecsale-mm CCH, including three materials on an Eulerian mesh. Fig. 11 (a) shows the volume fraction of the "shell" at different times. We can see that by 40 ns a jet of "shell" material has formed which is similar to a shaped charge jet. The corresponding density field is shown in Fig.11 (b). The peak density of the portion of the "shell" that has been compressed by the "high explosive", located behind the jet is approximately 8.5 g/cm^3. At 70 ns the velocity at the tip of the jet exceeds 90 cm/μs.

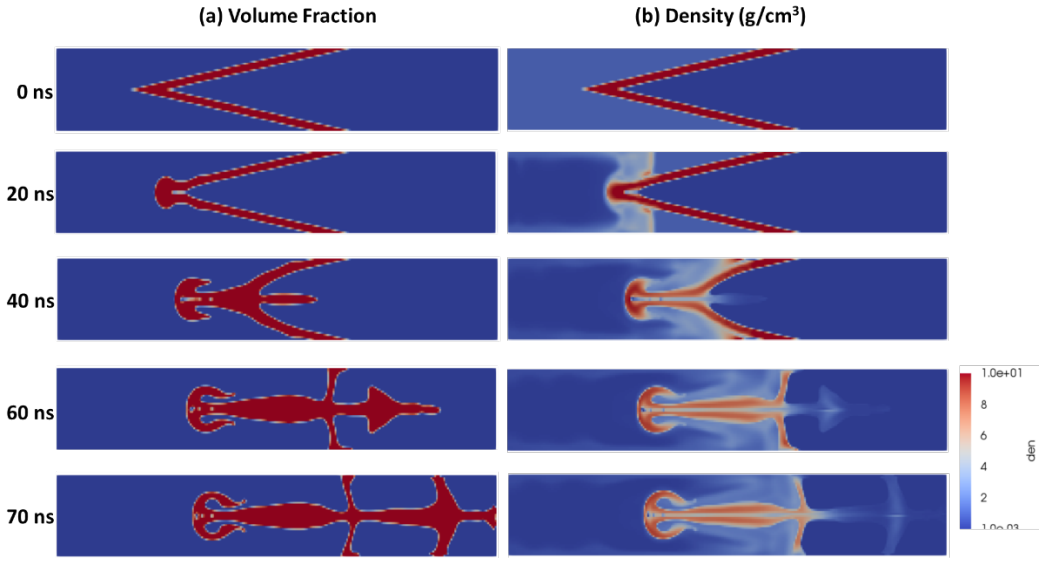

Figure 11. Results for the simplified shaped charge problem using the Flecsale-mm CCH app at various times during the simulation: (a) volume fraction of the projectile and (b) density.

9.0 Verney Shell Collapse

The Verney test problem [7] exercises material strength and was simulated with the Symphony SGH app on a purely Lagrangian mesh. This problem involves an isentropic imploding steel shell with an initial inner radius of 8 cm and a thickness of 0.5 cm. The initial velocity spatial profile is chosen to create a constant density implosion that converts the initial kinetic energy into internal energy. A simple strength model consisting of a constant shear modulus of 0.895 Mbar and a constant yield stress of 0.05

Mbar is used together with a Mie-Gruneisen equation of state for steel having the material parameters: ρ_0 = 7.90, C_0 = 0.457, S_1= 1.49, γ_0 = 1.93, and b = 0.50.

The shell is shown in Fig. 12 (a) at 0 μs (red) and 50 μs (blue) and the computational mesh represents an octant of the shell with just 5 cells in the radial direction. A total of about 64,000 cells comprise the octant with points smoothly distributed across the solid angle using an equipotential algorithm. At 50 μs the shell has almost completely collapsed and some hourglass distortion of the mesh is visible. This is not surprising given the extremely high aspect ratio of the cells at late time in the simulation.

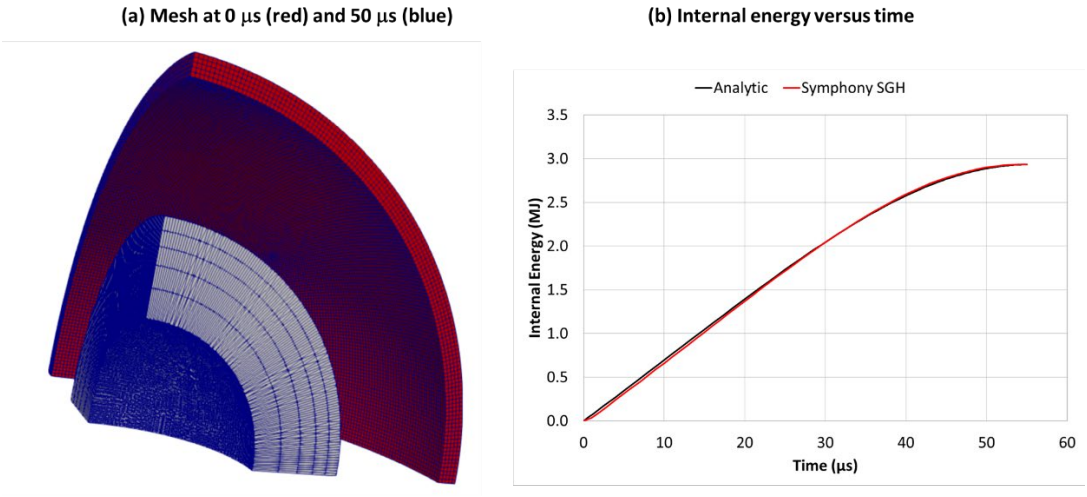

Figure 12. Simulation results for the Verney problem using the Symphony SGH app: (a) initial (red) and imploded (blue) computational meshes, and (b) internal energy of the shell versus time.

The internal energy of the steel shell as a function of time was derived using an analytical solution approach [7]. Computational results using the Symphony CCH app are compared with the analytical solution in Fig. 12(b). At stagnation time, which occurs near 55 μs, the calculated internal energy is virtually identical to the analytical solution on this very coarse mesh.

10.0 Taylor Anvil

The tantalum Taylor anvil test problem was simulated with the SGH method on a purely Lagrangian mesh, using both Flecsale-mm and FUEL. The SGH method was combined with the viscoplastic self-consistent (VPSC) model [5] to represent mesoscale crystal plasticity in the tantalum with high fidelity. In crystal plasticity models the distribution of crystal orientations, the available slip systems, and the stress levels necessary to activate them are taken into account explicitly, allowing for the evolution of anisotropy in the macroscopic stress field. The size of the grains and their initial orientations are taken as inputs, and at every subsequent cycle VPSC reorients the grains (i.e. updating the texture) using a homogenization scheme. The simulations of the tantalum experiment use grain texture information from a sample of 419 grains, and every cell in the simulation has 92,477 double variables worth of data associated with the VPSC model. The simulation of the tantalum Taylor anvil involves 5,148 cells.

The existing Fortran 90 VPSC code [8] and an existing C interface for the code were heavily modified in order to work with FLeCSI. These modifications included using C++ code to allocate the cell-centered, VPSC specific data that would normally be allocated by the Fortran 90 VPSC code. Furthermore new routines were added to the C interface, including one routine that copies the cell-centered, VPSC specific data from std::array objects, registered with FLeCSI, to the particular type of data structure that is passed into the Fortran 90 VPSC code. A corresponding routine copies the data back into the FLeCSI std::array objects after the VPSC call is complete. There is one VPSC call for every cell, at every cycle.

Fig. 13 shows calculated values of the (3,3) component of the Cauchy stress tensor within the tantalum at 10 μs from two different simulations with the SGH/VPSC algorithm using either Flecsale-mm or FUEL. The Flecsale-mm simulation used a single node of Snow with 32 processors. The FUEL simulation used 20 nodes of Snow with 520 processors. The two simulations are in excellent agreement. The rod is strongly in tension at the origin where the (3,3) component of Cauchy stress is -2500 MPa. As one moves radially away from the origin, the rod experiences compression with a peak value of about 400 MPa for the (3,3) component of Cauchy stress tensor on the outer surface of the rod. The initial outer radius of the rod is 3.81 mm. In the z=0 plane at 100 μs the FUEL simulation suggests an outer radius of about 8.5 mm in the y direction and 6.8 mm in the x direction, as shown in Fig. 14. The FUEL simulation produces an anisotropic stress field, and is in good agreement with the measured expansion of rod [9], whereas a simulation of the rod impact using the flecsale-mm CCH app with a PTW model for tantalum rather than the VPSC model does not capture the anisotropic nature of the stress and does not produce as much radial expansion in the y direction.

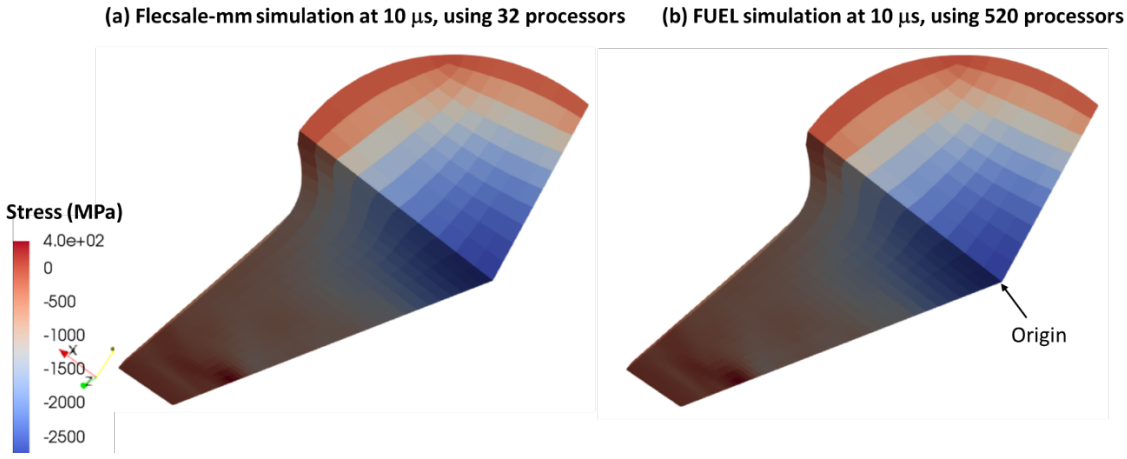

Figure 13. Calculated (3,3) component of Cauchy stress tensor for the Taylor Anvil problem at 10 μs: (a) using the Flecsale-mm SGH/VPSC app and (b) using FUEL with the SGH/VPSC method.

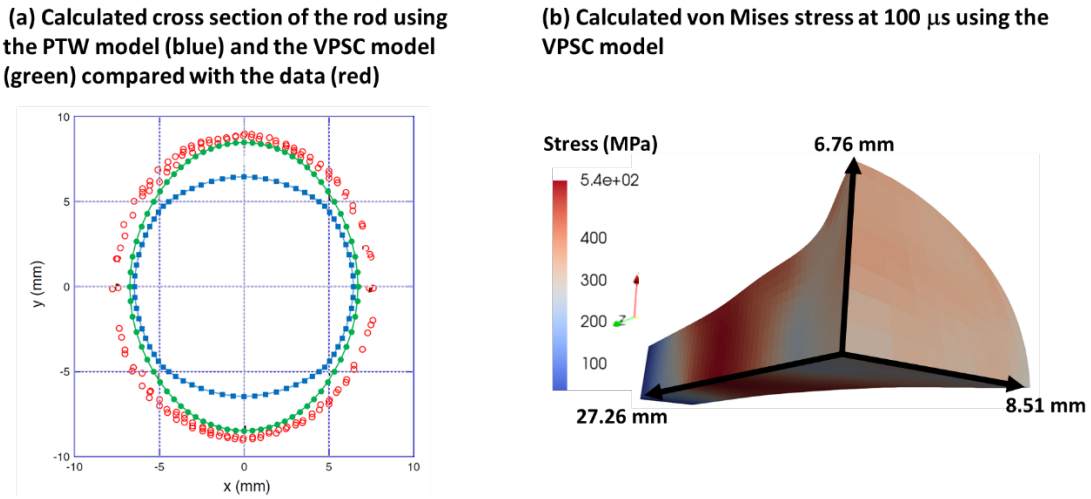

Figure 14. Simulation results for the Taylor Anvil problem at 100 μs: (a) cross section of the rod in the z=0 plane from the flecsale-mm CCH app using the PTW model (blue) and FUEL using the SGH/VPSC method (green) compared with data (red), and (b) von Mises stress from FUEL using the VPSC SGH/VPSC method. The figure with the data was taken from Ref. 9 and the calculation results were plotted on top of the figure.

11.0 5-Material Compression Problem

The 5-material problem has two steel cylinders that are separated by a high pressure gas region as shown in Fig. 15. The steel cylinders are driven by the high pressure gas [7]. This test problem has contact discontinuities, release waves, and shocks. A conformal mesh with 150 radial zones, 90 azimuthal zones, and 10 axial zones was created to simulate this problem. The outer steel cylinder has a thickness of 0.25 cm which is spanned by 10 radial zones and the inner shell is 0.5 cm thick with 40 radial zones. There are 10 axial zones in the problem and the cylinders are 5 cm long. The high pressure gas region depicted in Fig. 15 contains 80 radial zones and provides the energy to compress the inner steel cylinder and to expand the outer steel cylinder. Contained within the inner cylinder is a low pressure gas region consisting of 20 radial zones. Both gas regions were represented as ideal gases in simulations and were initialized according to the conditions specified in Fig. 15. Both steel cylinders are represented by a Mie-Gruneisen equation of state and an elastic, perfectly-plastic constitutive model. This test problem is simulated to a time of 5 μs.

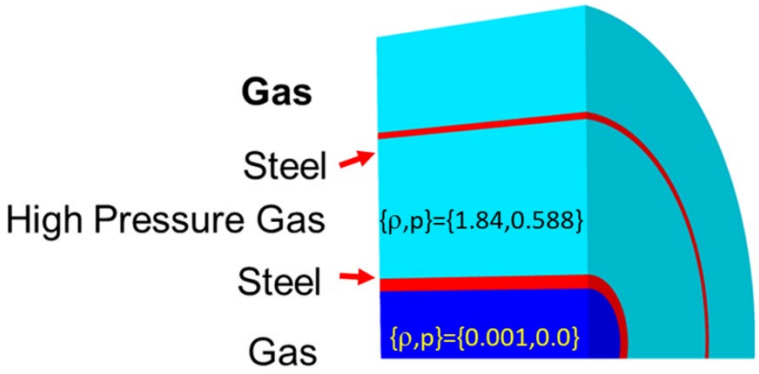

Figure 15. The geometry of the 5-material compression problem.

Two kinds of Eulerian 3D calculations are performed using the Symphony CCH app with both the multi-material remap and the IA-SSD closure model: one calculation with the computational mesh described above, consisting of 150 by 90 by 10 cells, where the mesh lines in the x-y plane are conformal with the initial contours of the steel cylinders, and another calculation where the mesh lines have uniform spacing in the x-y plane, consisting of 200 by 200 by 10 cells. For calculations with the uniform Eulerian mesh, the reconstruction of stress and velocity values in the cell corners used linear reconstructions within the CCH algorithm as opposed to quadratic reconstructions. In addition to the two calculations with the Symphony CCH app, a companion calculation on the conformal mesh was also performed with the Symphony SGH app. For further comparison, a pure Lagrangian calculation was performed with FLAG, in 2D axially symmetric geometry. All four simulations give a total energy (internal plus kinetic) of about 2.7 MJ for the inner steel cylinder at 5 μs. The internal energy calculated during the compression of the inner steel cylinder is presented in Fig. 16. There is excellent agreement between the Symphony CCH and SGH apps for the internal energy as a function of time. Both CCH and SGH apps agree fairly well with the 2D axially symmetric Lagrangian calculation.

The calculated (1,1) component of the deviatoric stress at 5 μs is shown in Fig.17, using the Symphony CCH app with three different computational approaches: (1) a pure Lagrangian simulation on the conformal mesh (150 by 90 by 10 cells), (2) a pure Eulerian simulation on the conformal mesh, and (3) a pure Eulerian simulation on the uniform mesh (200 by 200 by 10 cells). The stress field is virtually identical using any of the three computational approaches. This indicates that the multi-material remap introduces a relatively small amount of diffusion at the interfaces between different materials, and does not artificially distort the stress field. Furthermore, the fact the Symphony CCH app gives essentially the same result for the (1,1) component of the deviatoric stress using either the conformal or uniform mesh indicates that the multi-material remap is fairly accurate even when the hydrodynamic flow is not aligned with the mesh.

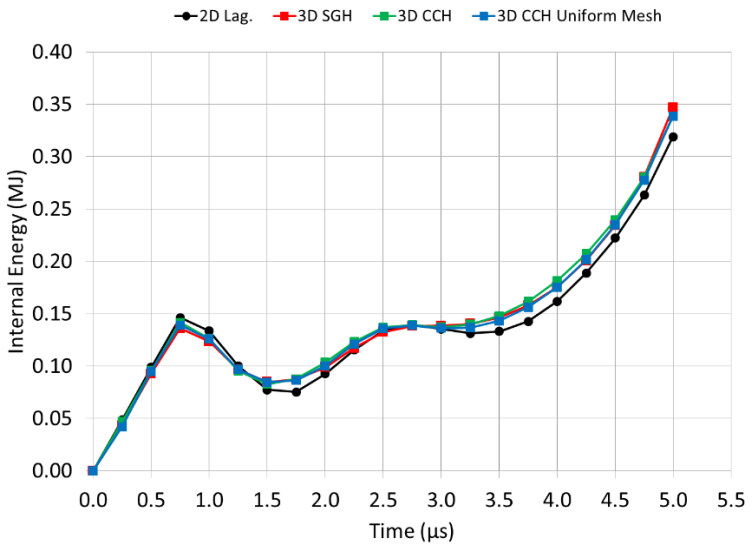

Figure 16. Symphony simulation results for the internal energy of the inner steel shell using four different methods: (green) CCH with conformal Eulerian mesh, (blue) CCH with uniform Eulerian mesh, (red) SGH with Eulerian mesh, and (black) 2D SGH pure Lagrange. All of the Eulerian calculations use the multi-material remap with interface reconstruction and the IA-SSD closure model.

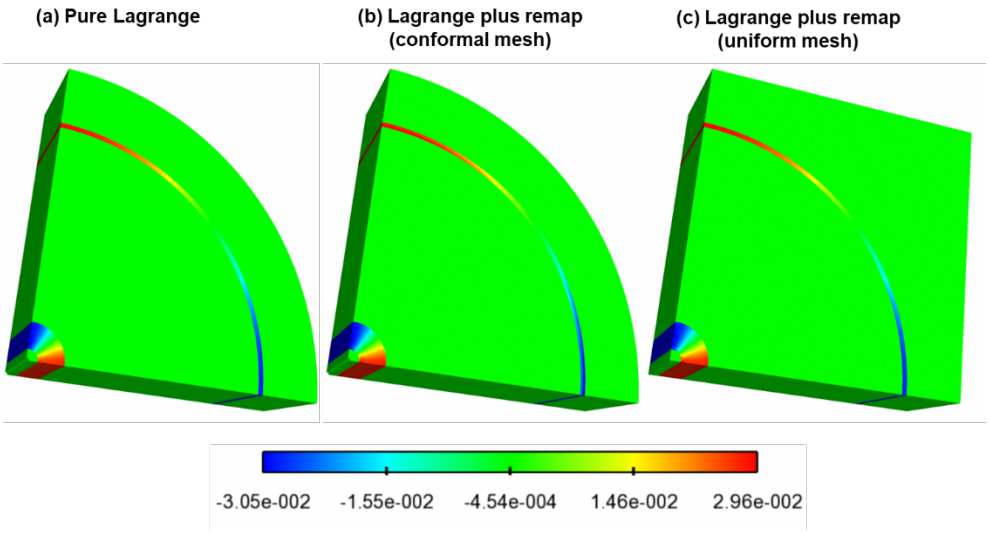

Figure 17. Contours of the (1,1) component of the deviatoric stress tensor at 5 μs using the Symphony CCH app with three different computational approaches: (a) pure Lagrange, (b) pure Eulerian on a conformal mesh, and (c) pure Eulerian on a uniform mesh. Both of the Eulerian calculations use the multi-material remap with interface reconstruction and the IA-SSD closure model. Material polygons including both hexahedral and tetrahedral elements are plotted.

In addition to the Symphony CCH calculations a larger Eulerian calculation was performed with FUEL using the conformal mesh, but increasing the number of zones in the axial direction from 10 to 100, resulting in 1.35 million zones. This problem was simulated on Snow using 10 nodes with 360 processors. In Fig. 18 the FUEL simulation results are compared with the corresponding results from the Symphony CCH app.

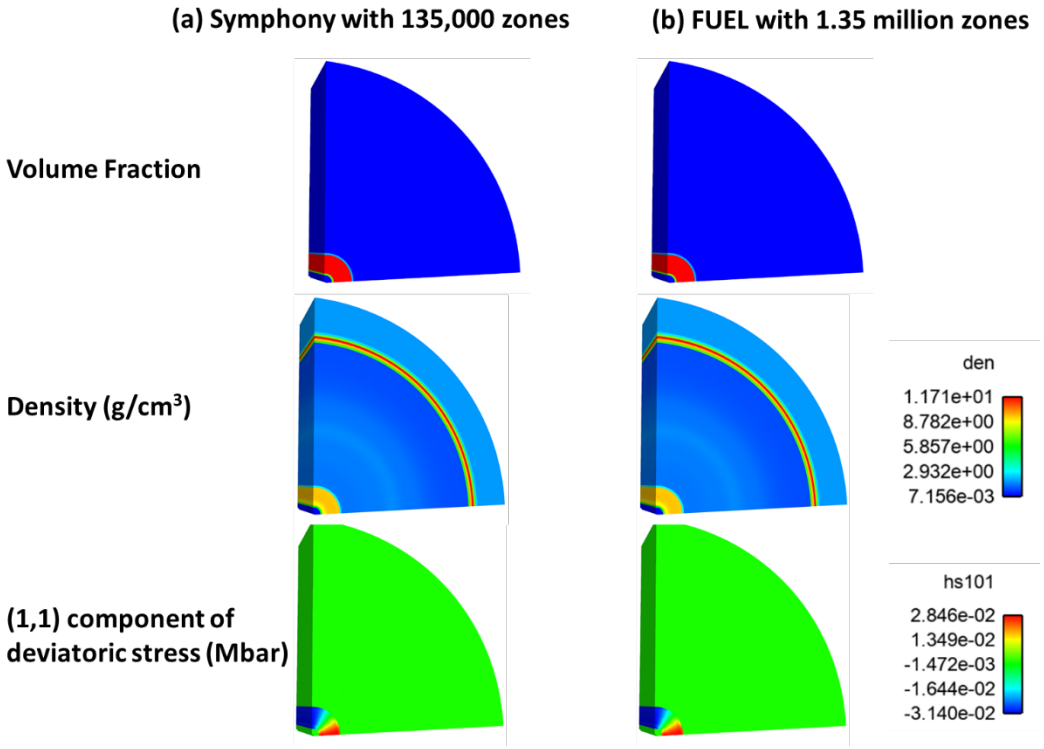

Figure 18. Comparison of Symphony CCH and FUEL results for the 5-material compression problem at 5 μs, showing computed values of volume fraction, density, and deviatoric stress.

12.0 Tin Pulsed Power Experiment

The final test problem involves a tin pulsed power experiment [10]. This is a Z-pinch experiment where a radial velocity of about 3 km/s is imparted to an aluminum cylindrical linear, using electromagnetic forces. The linear then collapses onto a hollow cylindrical tin target. The tin target has sinusoidal perturbations imprinted onto its inner surface which seed RM instabilities at late time in the experiment. There are three regions of the inner surface where surface perturbations are imposed, and the amplitude of the perturbations is different for each of the three regions. Proton radiography was used to interrogate the compressed state of the tin at multiple times and determine the growth rate of the amplitude of the RM features. The geometry of the experiment is illustrated in Fig. 19.

A 2D Cartesian FLAG model of the experiment was created using ingen to create a conformal mesh of the tin, including the surface perturbations, as well as the central gas region contained within the inner surface of the tin cylinder. There is a slide line between the inner surface of the liner and the outer surface of the tin. An initial uniform radial velocity of 3 km/s was specified within the liner. At about 3 μs the liner impacts the tin target, and at 3.2 μs a 2D trilink file is created which is subsequently used as input for Eulerian simulations with the Flecsale-mm CCH app and FUEL.

(a) Illustration taken from LA-UR-17-24720, showing the liner and target in the Z-Pinch experiment

(b) Illustration taken from LA-UR-16-26208, showing the cross section of the Z-Pinch experiment

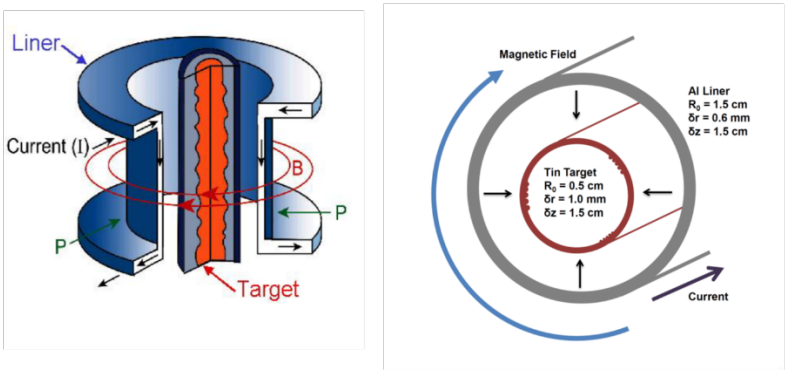

Figure 19. The geometry of the tin Z-pinch experiment, showing the orientation of the current and magnetic field in the liner (a), and a cross section of the tin target with perturbations on its inner surface (b).

The 2D trilink file was read by Flecsale-mm and the 2D triangular elements were mapped onto a uniform Eulerian mesh and extruded to create a 3D geometry, including four materials: background gas, liner, tin target, and central gas region. The resulting 3D mesh consisted of 330 by 330 by 2 cells. A simple elastic, perfectly plastic strength model and a Mie-Gruneisen equation of state were used to represent both the liner and the tin, with separate parameters appropriate for each material. Fig. 20 compares the calculated densities in the simulation at three separate times near stagnation, to the measured proton radiographs. In order to compare radiograph and Flecsale-mm CCH simulation, the simulation results were shifted in time by -0.2 μs, and spatially scaled to approximately match the area of the shocked tin region visible in the radiograph. The behavior in the liner is different in the simulation than in the radiographs. There is much more outward radial expansion of the aluminum liner in the simulation than what is suggested in the radiographs. The simulated shape of the collapsed tin, especially the imprinting of the inner surface perturbation onto the outer surface of the tin, corresponds well to what is observed in the radiographs. The collapsed/shocked tin region has a density of roughly 7.1 g/cm^3, which is slightly less than nominal tin density. There is a halo of lower density (~3.0 g/cm^3) tin that surrounds the collapsed/shocked region.

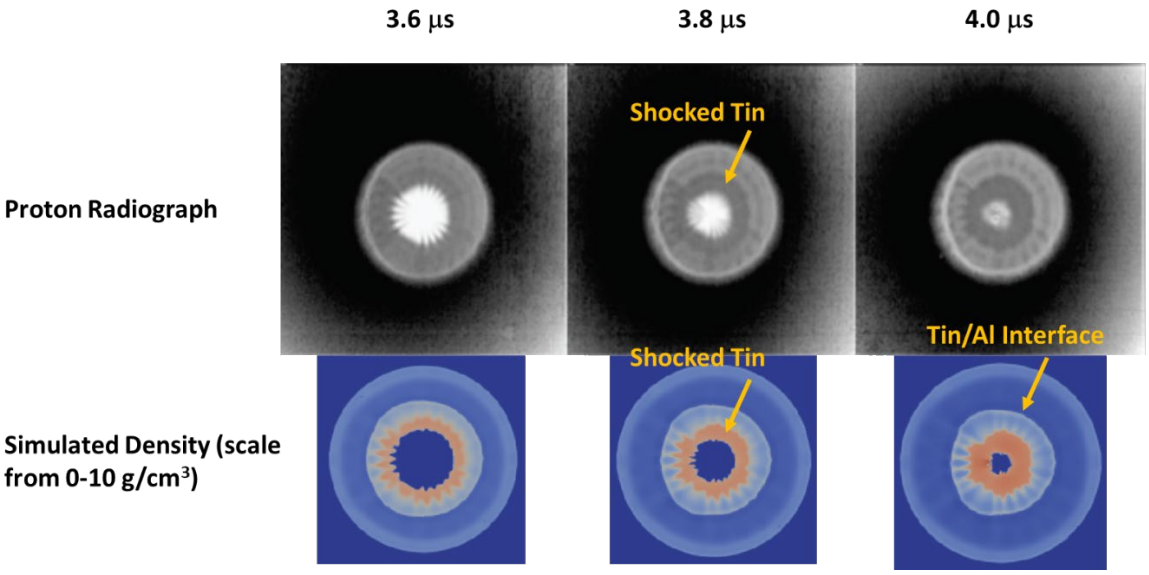

Figure 20. Comparison of Flecsale-mm CCH simulation results for the tin Z-pinch experiment with the measured proton radiographs.

In addition to the Flecsale-mm simulation, a separate calculation was also performed with FUEL using the same mesh and initialization procedure, but with a more sophisticated PTW strength model for the tin. With this model the equivalent plastic strain was calculated at every cycle and used to update the yield stress of the tin. The equivalent plastic strain was also updated during the remap step, as tin was being moved across the mesh. Fig. 21 indicates that the inclusion of the PTW model does not change the calculated densities in the collapsed/shocked tin region in any appreciable way.

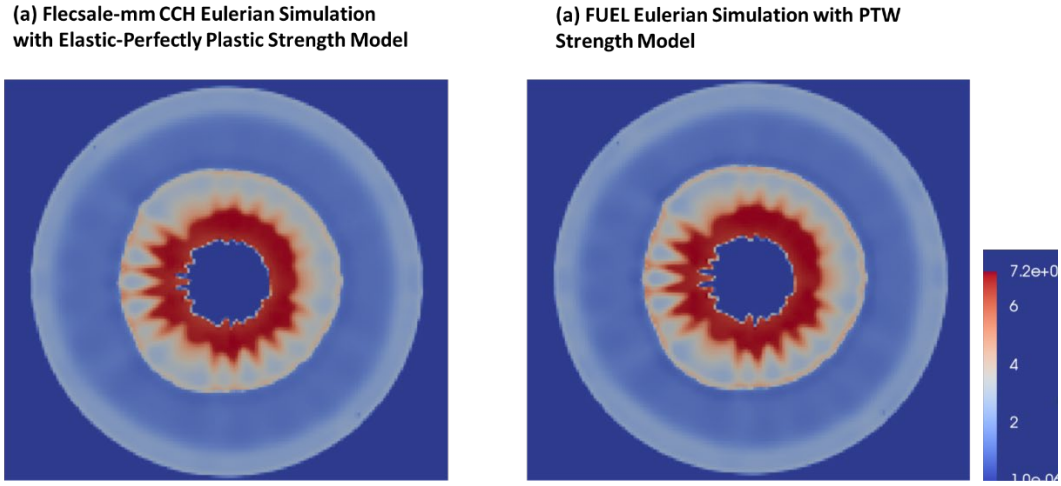

Figure 21. Comparison of calculated densities from a Flecsale-mm CCH simulation with an elastic, perfectly plastic strength model for tin and from a FUEL simulation having a PTW model for tin. The simulation time corresponds to a radiograph time of 3.8 μs.

References

1. Vincent P. Chiravalle, Andrew Barlow, and Nathaniel R. Morgan, “3D Cell-Centered Hydrodynamics with Subscale Closure Model and Multi-Material Remap,” Computers and Fluids 207, Article 104592, 2020.
2. Vincent P. Chiravalle, and Nathaniel R. Morgan, “A 3D Finite Element ALE Method using an Approximate Riemann Solution,” International Journal for Numerical Methods in Fluids 83, p. 642-663, 2017.
3. Vincent P. Chiravalle and Nathaniel R. Morgan, “Multi-Material Arbitrary Lagrange-Eulerian Methods for Hydrodynamics in Three Dimensions,” Los Alamos National Laboratory Report LA-UR-19-20334, 2019.
4. A. Barlow, M. Klima, M. Shashkov, “Constrained Optimization Framework for Interface-Aware Sub-Scale Dynamics Models for Voids Closure in Lagrangian Hydrodynamics,” Journal of Computational Physics 371, p. 914—944, 2018.
5. R. A. Lebensohn, C. N. Tome, and P. Ponte Castaneda, “Self-consistent modelling of the mechanical behaviour of viscoplastic polycrystals incorporating intragranular field fluctuations,” Philosophical Magazine 87, p. 4287-4322, 2007.
6. S. D. Ramsey, L. S. Brown, E. M. Nelson, and M. L. Alme, A Class of Self-Similar Hydrodynamics Test Problems, Los Alamos National Laboratory Report LA-UR-10-08184, 2010.
7. Vincent P. Chiravalle, “Cercion: A Material Strength ALE Code with a Higher-Order Remap using Flux Volume Centroids,” Los Alamos National Laboratory Report LA-UR 12-00799, 2012.
8. R. A. Lebensohn, Viscoplastic Fast Fourier Transform-based (VPFFT) code, version 1, Los Alamos National Laboratory LA-CC-11-003, 2011.
9. B. Plunkett, O. Cazacu, R. A. Lebensohn , and F. Barlat, “Elastic-viscoplastic anisotropic modeling of textured metals and validation using the Taylor cylinder impact test,” International Journal of Plasticity 23, p. 1001–1021, 2007.
10. C. L. Rousculp, D.M Oro, J.T. Bradley, J.R. Griego, M. Freeman, R.E. Reinovsky, P.J. Turchi, and W.A. Reass, “Crenulation-1 Flash Report,” Los Alamos National Laboratory Report LA-UR-16-26208, 2016.